



# Loads and response on flexible conical and cylindrical fish cages: A numerical and experimental study based on full-scale values

Per Christian Endresen<sup>\*</sup>, Pascal Klebert

SINTEF Ocean, Seafood Technology, Aquaculture Structures, Postboks 4762 Torgarden, 7465, Trondheim, Norway

## ARTICLE INFO

**Keywords:**  
 Aquaculture  
 Fish cages  
 Deformation  
 Drag forces  
 Numerical simulation

## ABSTRACT

This paper presents drag forces from uniform water current on two flexible net cage designs, commonly used in Norwegian fish farming, obtained through model-scale testing and numerical simulations. The primary focus is on the comparison between model tests and numerical simulations and performance of the numerical model for the different net cage designs. The two designs were a cage with a cylindrical main section with straight walls and conical bottom with a sinker tube weight system and a cage where both the main section and bottom has a conical shape. The latter cage has a central weight instead of a sinker tube. The effect of the governing parameters was explored by varying the design and loads of the weighting system. Both physical tests and numerical simulations revealed increased drag forces and reduced ability for deformation when increasing the load from the weighting system. Lower weight system load or weight system designs that allow for more deformation decrease the loads on the net cage. Although it was not a focus in the present work, fish welfare is dependent on sufficient available volume in the net cage, meaning that large reductions in volume to reduce drag forces at high current velocities may be undesirable. Comparisons between model scale tests and numerical simulations reveal good agreements for the highest weight system loads tested. Decreasing the weight system loads decrease the accuracy of the numerical simulations. This may be caused by larger deformations of the net cage when the bottom loads are reduced resulting in a larger number of net panels with small angles of attack relative to the incident current. Predictions of forces for low angles of attack may be less accurate than for larger angles of attack while there is a possibility of increased flow velocity reduction (wake effect) and flow deflection. The cages were tested and simulated for flow velocities up to 1.25 m/s (full scale value). Measurements of the flow velocity in the middle of the net cages revealed a higher velocity reduction than predicted with theory, with the exception of the highest velocity.

## 1. Introduction

The United Nations Food and Agriculture Organization (FAO, 2018) issued a report stating that aquaculture, with a 5.8% annual growth rate since 2010, continues to grow faster than other major food production sectors. One trend is the development of aquaculture production at offshore sites that are more exposed to currents and waves. In this context, the sea cage is a new fishing concept based on floating, flexible, and circular gravity cages, which are the most widely used, or completely new net-based farming systems.

In the past, several experiments have been carried out to investigate the hydrodynamic characteristics of net cages and structures (e.g. Løland (1991), Zhan et al. (2006), Balash et al. (2009) and Patursson et al. (2010)). A review can be found in Klebert et al. (2013). Studies on

net panels or net cages can further be used for development of numerical models for hydrodynamic forces on nets and net cages. These may be categorized into two approaches: 1) the Morison-type force model and 2) the screen model. In the Morison-type force model, nets are modeled as individual twines. But, due to the large number of twines in net cages, the physical net cage may be represented by an equivalent mesh system with fewer twines. A Morison-type model is then applied to calculate the forces on each twine (see, for example, Li et al., 2006; Moe et al., 2010). In the screen model the net is divided into a number of panels, each subjected to a force dependent, among others, on the orientation of the entire panel. A Morison-type model typically focus on individual twines for calculation of hydrodynamic loading while a screen-type model focus on the panel. Hybrid models, where the net is divided into panels, while hydrodynamic force calculations are based on the orientation of

\* Corresponding author.

E-mail address: [Per.Christian.Endresen@sintef.no](mailto:Per.Christian.Endresen@sintef.no) (P.C. Endresen).

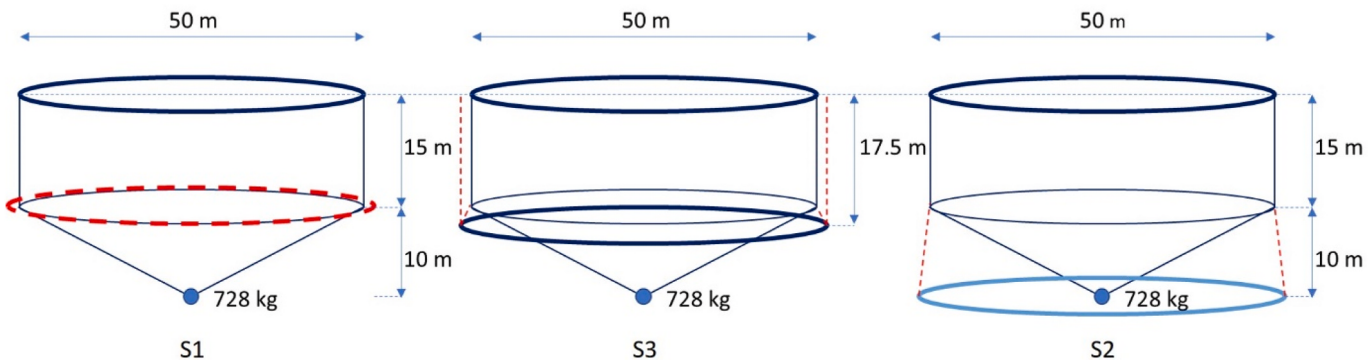


**Fig. 1.** Schematic diagrams of the bottom ring setup of the cylindrical cage. The red dashed ring represents the integrated bottom ring. The dark and light blue rings represent the supported floating collar and the suspended net-supported ring, respectively. The red dashed lines are the lines supporting the bottom ring. All masses are wet weights. The bottom ring circumference and wet weight are 160.9 m and 91 kg/m, respectively. (For interpretation of the references to color in this figure legend, the reader is referred to the Web version of this article.)

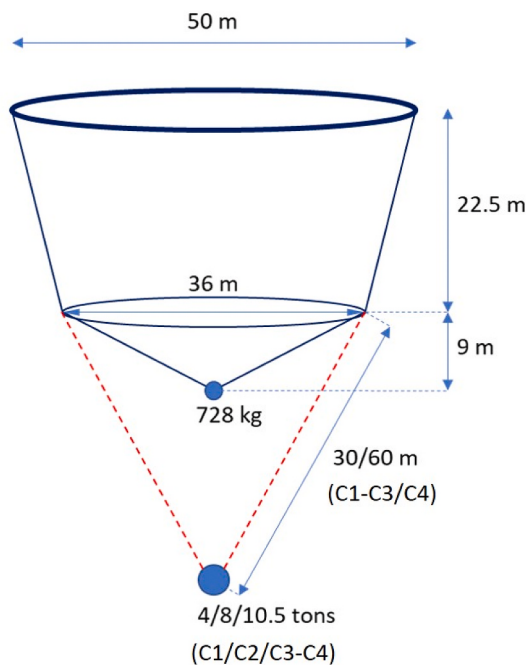


**Fig. 2.** Schematic diagram of the conical cage weight setup. Four different setups were tested, including 3 central weights and 2 supporting rope lengths (red dashed lines). All weights are wet weights. Weight of the central load in metric tons. (For interpretation of the references to color in this figure legend, the reader is referred to the Web version of this article.)

the twines (equal along each individual panel) also exists (Endresen et al., 2014). For all methods the resulting force is usually decomposed into a drag force and a lift force. Both main types of models may or may not include wake effect considerations, i.e. parts of the net shielded by upstream parts of the net in steady currents. Studies on shielding and the flow field inside and around net cages include Løland (1991), Patursson et al. (2010), Gansel et al. (2012) and Zhao et al. (2015). Both methods usually consider solidity directly or indirectly, and in some instances effect of knots. A Morison-type force model may overestimate forces for low angles of attack, e.g. when the inflow direction goes towards parallel with the net panel partly due to self shielding from adjacent parts of the net. Løland (1991) derived a screen model where the drag and lift force coefficients were found and validated by data from laboratory tests on net panels. The tests involved variation in netting solidity and angle of attack and included wake effect considerations. Kristiansen and Faltinsen (2012) used a theoretical and semi-empirical approach to derive a

**Table 1**

Overview of net cage designs (shape, weighting and suspension method). Bottom weights (metric tons) and suspension rope lengths given in full scale values.

Case	Net type	Weighting	Weight suspension
S1	Cylindrical	Bottom ring, net cone weight	Integrated, supported by the net
S2	Cylindrical	Bottom ring, net cone weight	Suspended 10m below net, supported by the net
S3	Cylindrical	Bottom ring, net cone weight	Suspended from the collar
C1	Conical	Suspended center weight, net cone weight	Suspension ropes 60 m, weight 4 T
C2	Conical	Suspended center weight, net cone weight	Suspension ropes 60 m, weight 8 T
C3	Conical	Suspended center weight, net cone weight	Suspension ropes 60 m, weight 10.5 T
C4	Conical	Suspended center weight, net cone weight	Suspension ropes 30 m, weight 10.5 T

screen force model. The model was compared with model test data. A difference from Løland (1991) is the addition of Reynolds number dependency on the drag coefficient and the possibility of using a second harmonic function ( $\cos(3\theta)$  and  $\sin(4\theta)$ , dependent on panel normal angle ( $\theta$ ) to the current) for determining the shape of the drag and lift coefficient function for each net panel, respectively. The drag and lift formulations from Kristiansen and Faltinsen (2012) were integrated in SINTEF Oceans in-house software FhSim. It was used to assess the ability to obtain full-scale estimates of forces on aquaculture net cages by comparing its performance to up-scaled model-scale experiments. This numerical model uses established methods for the evaluation of hydrodynamic loads on and structural forces in the netting material, enabling verification against previously published works that have modeled current forces on aquaculture net cages.

In the present study, the drag forces obtained for various net cage designs exposed to uniform water current in model scale experiments in a towing tank are presented, and the results are compared with numerical simulations. The experiments included two separate net cage designs: a) Cylindrical main section with vertical walls, a conical bottom and sinker tube weight system (Fig. 1) and b) Conical design with slanted walls, a conical bottom and a central weight (Fig. 2).

## 2. Materials and methods

### 2.1. Experimental setup

The two fish cage models (Figs. 1 and 2 and Table 1) were tested by towing of scaled models (scale 1:25) with constant velocities. The water velocities and forces were measured while the deformation experienced

**Table 2**

Model/Full scale values of net cage setup. Loads scaled in the same manner as for Froude scaling (scale 1:25).

Parameter	Unit	Cylindrical (S1 – S3)	Conical (C1 – C4)
Diameter top	m	2/50	2/50
Diameter bottom	m	2/50	1.44/36
Height main part	m	0.6/15	0.9/22.5
Height cone	m	0.4/10	0.36/9
Sn (solidity)	–	0.245/0.245	0.245/0.245
Twine diameter	mm	-/2.62	-/2.62
Half mesh width	mm	6.3/20	6.3/20
Cone weight (submerged)	kg	0.045/728	0.045/728
Central suspended weight (submerged)	kg/ $10^3$ kg	–	0.25/4, 0.50/8, 0.66/10.5
FhSim E-modulus	Pa	-/2·10 <sup>8</sup>	-/2·10 <sup>8</sup>

by the cages were assessed qualitatively with a video camera. Assuming similar magnitudes for the drag coefficient for the net for model and full scale it can be shown that forces and velocities can be scaled in the same manner as for Froude scaling. Model and full scale dimensions for the two net cage designs can be found in [Table 2](#). Netting parameters are described in section 2.3. The cylinder-shaped net ([Fig. 1](#)) had a sinker tube type weight system with a central weight in the bottom of the net cone, while the cone-shaped net cage ([Fig. 2](#)) had two central loads. One of these loads was connected to the net cone bottom, while the heaviest weight was connected to the bottom perimeter of the upper conical part of the net by long suspension ropes. The vertical position and attachment method of the sinker tube of the cylindrical net and the vertical position of the main load weight of the conical cage were varied along with the magnitude of the selected weights to assess how the net cage designs reacted to water currents. The main geometry of the net cage and floating collar and sinker tube was geometrically scaled. The diameter of the floating collar cross section was, however, slightly larger than the diameter of floating collars commonly used today for flexible gravity-type net cages due to the decision to use one floating collar instead of two.

## 2.2. Weights

For the cone-shaped cage, three different bottom weights were used and assessed in addition to two different suspension rope lengths ([Fig. 2](#)). For the cylinder-shaped cage, only one bottom ring weight was used in the three different configurations: integrated in the net, suspended from the bottom of the net, and suspended from the collar at the

surface ([Fig. 1](#)). All cases are summarized with case numbers in [Table 1](#).

## 2.3. Net model

The twine diameter and half mesh width of the netting were not scaled geometrically, as this would not have been feasible due to the resulting small diameter and length of the mesh bars in the netting. Instead, model nets with a smaller thread diameter and mesh bar length than the full-scale equivalent were used while maintaining the same solidity ratio as the full-scale netting material. Solidity is defined as the ratio between the projected area of the netting material and the total area of the net panel. The two most common formulas used to determine netting solidity are  $Sn = 2d/l$  and  $Sn = 2d/l - (d/l)^2$  where  $d$  and  $l$  are the mesh bar diameter and length, respectively. The latter formula evaluates the netting as an idealized structure consisting of crossing circular cylinders, while the former may better account for the extra material often found in the knots of aquaculture netting. The netting material used in the experiments has a measured half mesh (mesh bar length) of approximately 6.3 mm. The twine diameter could not be reliably measured. To assess the solidity, image analysis was applied. A threshold was used to generate a two-color image, for which an average solidity of 0.245 was obtained ([Fig. 3](#)). It should be noted that the measured half mesh and solidity cannot be used to derive the actual twine diameter as per standard formulas for estimation of solidity based on twine diameter and half mesh size due to the structure of the knots and the added projected area it produces. Although the term knot is used for the intersections between the twines the netting material has a Raschel knitting pattern, meaning that the net does not have conventional knots.

## 2.4. Test facilities and force measurements

The tests were conducted in the Bulgarian Ship Hydrodynamics Centre in Varna, Bulgaria. The tests were run in a towing tank with a length, width, and depth of 200 m, 16 m, and 6.5 m, respectively. The floating collar and net cages were connected to the tank's towing carriage through a horizontal mooring system ([Fig. 4](#), [Fig. 5](#)), thus simulating water current through towing of the model. The accuracy of the velocity measurements on the carriage was 1 mm/s in rms values.

Drag forces on the floating collar and net structure were measured by two HBM U9B 100 N force transducers (one upstream of the structure and one downstream) connected to ropes parallel to the towing direction. These ropes were connected to bridles attached to the fore and aft ends of the floating collar ([Fig. 5](#)). The alignment of the mooring lines

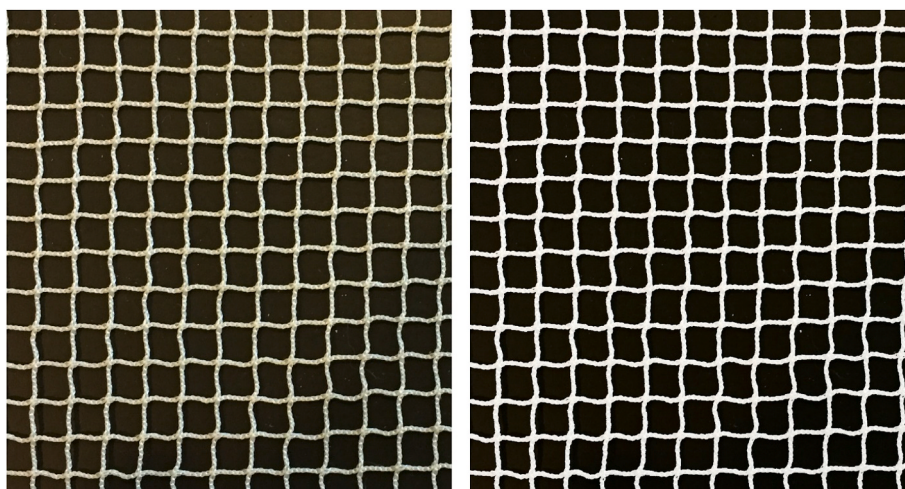


**Fig. 3.** Picture of the model scale netting used in the model tests (left) and the two-color digital image (right). The ratio between the white pixels and total number of pixels determines the solidity (0.245). The half mesh width was determined to be 6.3 mm.

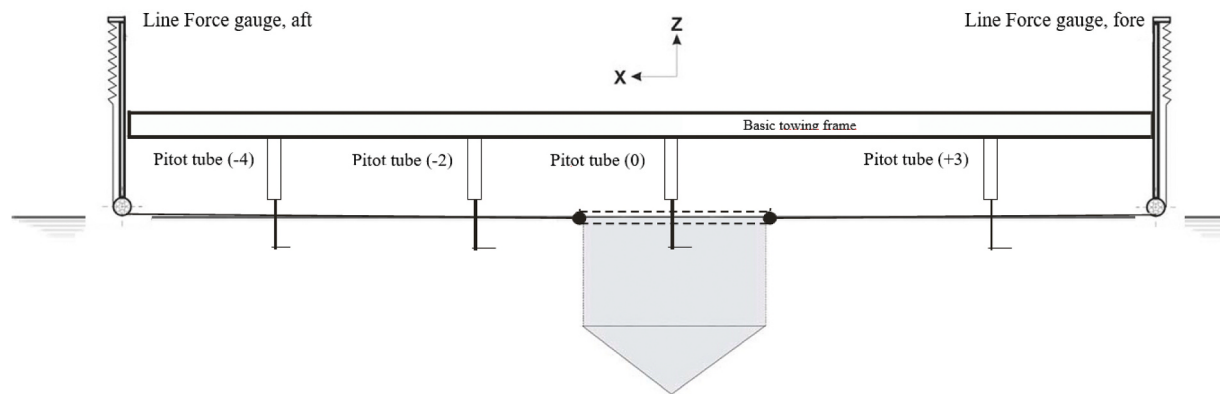


Fig. 4. Side view of test setup.

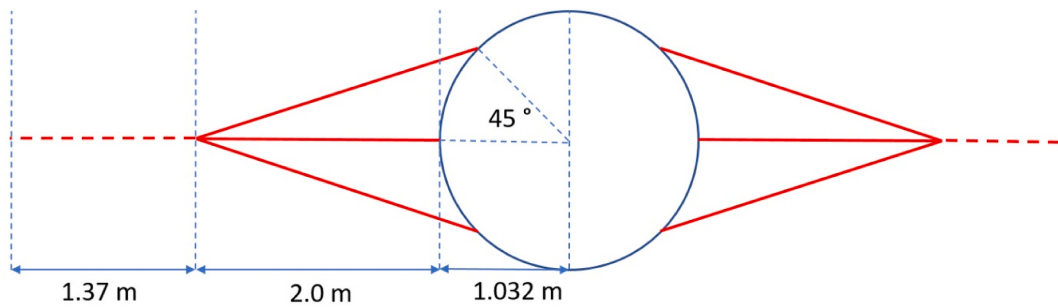


Fig. 5. Top view of test setup (floater and mooring). The diameter of the net attached on the inside of the floating collar is 2.0 m. Measurements were made from the outside of the ring.

**Table 3**  
Simulated bottom ring parameters (full scale).

Parameter	Unit	Cylindrical (S1 – S3)
Circumference	m	160.9
Section diameter	m	0.28
Wet weight	kg/m	91
EI (bending stiffness)	Nm <sup>2</sup>	365.7·10 <sup>3</sup>

**Table 4**  
Cable dimensions and material properties used in the numerical model (full scale).

Properties	Cross section diameter	Length	E-modulus	Mass per meter (dry weight)
Unit	m	m	Nm <sup>2</sup>	kg/m
Cone central weight ropes (C1–C4)	0.02	60/60/ 60/30	1·10 <sup>9</sup>	0.322
Sinker tube to surface support ropes (S3)	0.02	17,5	2·10 <sup>9</sup>	0.353
Sinker tube to net connection ropes (S1–S3)	0.02	-/10/ 2.573	1·10 <sup>9</sup>	0.353

ensured that the drag forces on the structure could be measured directly as the difference between the inline forces measured by the strain gauges. The transducers have an accuracy class of 0.5, with a range of 0–100 N.

Drag force measurements were obtained by towing the model through the tank at a variety of constant velocities. The mooring lines were pretensioned to 65 kN (full scale value), while a rope was stretched between the front (upstream) and aft (downstream) part of the floating collar. Due to the flexibility of the floating collar, it was necessary to

avoid excessive horizontal deformations, which affect the drag forces by altering the shape of the net cage. Forcing the shape of the floating collar significantly reduce the impact on the net from horizontal deformations of the floating collar while also negating the effect of having only two bridles attached in-line with the towing direction.

## 2.5. Numerical simulation setup

SINTEF Ocean's in-house software FhSim (Reite et al., 2014; Su et al., 2019) was used to numerically simulate the model test setups in full scale. FhSim is a software platform and framework for mathematical modeling and numerical simulation with a focus on marine applications. As only constant water velocities were assessed, the numerical setup was simplified. The net, ropes fixed to the sinker tube and the central weight (conical net cage), weights and the sinker tube (cylindrical net cage) were modeled, while the floating collar and bridles were not included in the model. This simplification is equivalent to a floating collar that perfectly holds its shape (circle). While this is only an approximation, it was deemed appropriate for the cases investigated. It will also reduce uncertainties in the simulations by reduction of parameters. The sinker tube was modeled as a cable with resistance to axial, bending, and torsional deformations (Table 3), while all ropes were modeled as cables with negligible bending stiffness (Table 4).

The net was modeled with triangular Priour structural elements Priour (1999) by connecting the vertices to form a complete net structure with sides (vertical or slanted) and a conical bottom. Hydrodynamic forces on the net elements were estimated using the screen type model formulated by Kristiansen and Faltinsen (2012). The net, cables, and sinker tube are connected by constraints (position) or applied force for each timestep in the simulation. Further references on FhSim, structural models, connections between elements in the model, and time integrations schemes can be found in Su et al. (2019), Endresen et al. (2014) and Reite et al. (2014). The net cage geometry was realized by

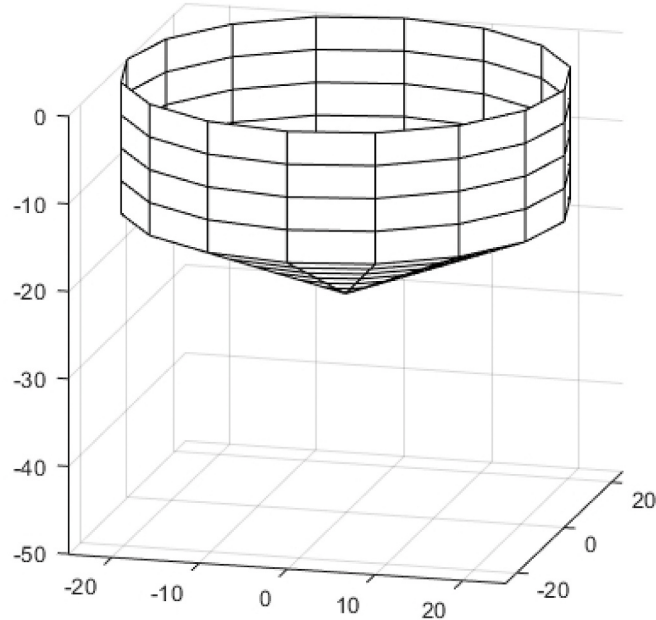


**Fig. 6.** Cylindrical cage (canonical view, numerical model). The square elements represent the discretization of the net and are further divided into triangles. Axes dimensions in meters.

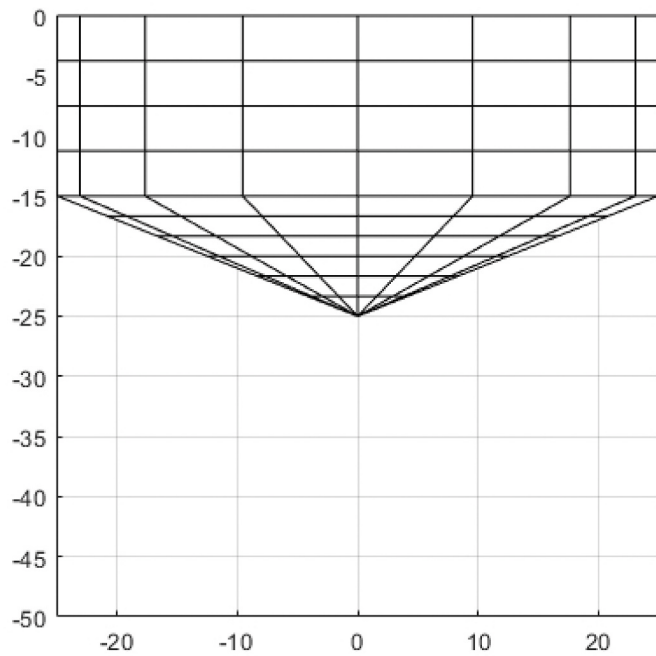


**Fig. 7.** Cylindrical cage (side view, numerical model). Top and bottom diameter = 50 m. Side wall and bottom cone heights = 15 m and 10 m, respectively. The square elements represent the discretization of the net and are further divided into triangles. Axes dimensions in meters.

dividing the net cage into a set number of four-sided surfaces each divided into two triangular panels. The cylindrical net structure has  $16 \times 4 \times 6$  four sided elements distribution along the circumference, vertical walls and radially in the bottom, respectively (Fig. 6, Fig. 7). The distribution is  $16 \times 5 \times 6$  for the conical net structure (Fig. 8, Fig. 9). This yields a total number of 762 and 960 triangular elements for the cylindrical and conical cases, respectively.

The twine diameter and half mesh length were set to 2.62 mm and

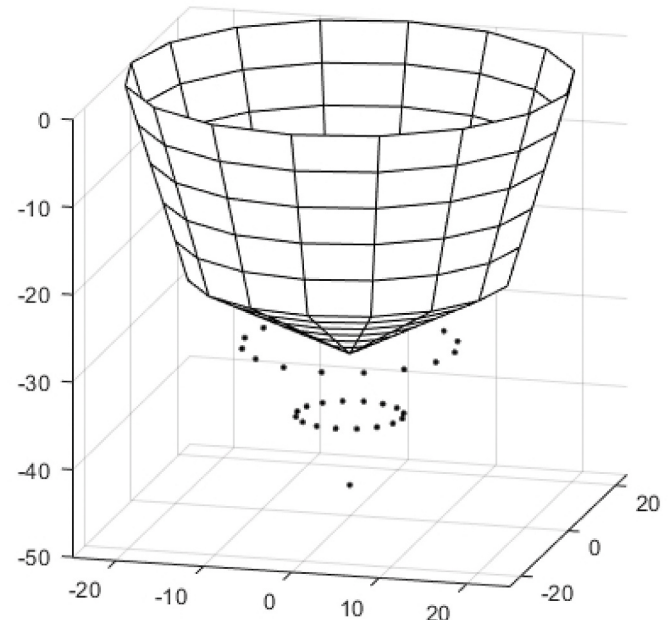


**Fig. 8.** Conical cage (canonical view, numerical model). Dots represent the nodes of the cables used to model the short suspension ropes (30 m) for the central weight. The square elements represent the discretization of the net and are further divided into triangles. Axes dimensions in meters.

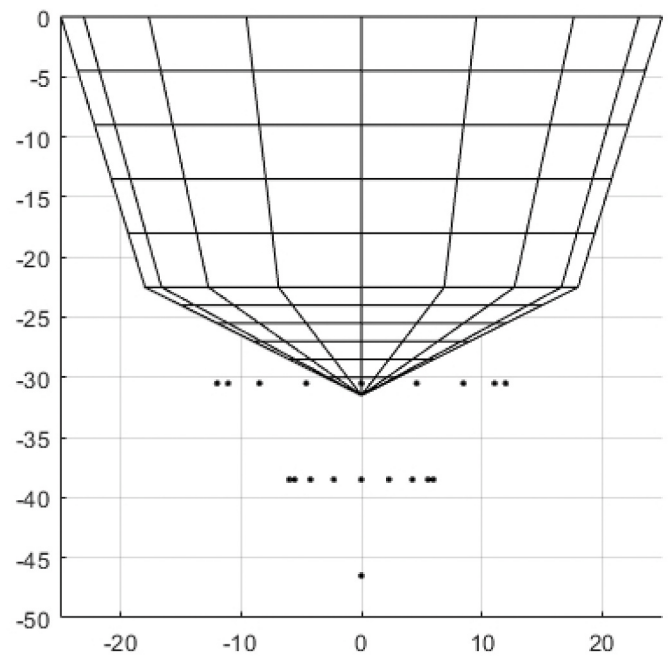


**Fig. 9.** Conical cage (side view, numerical model). Top and bottom diameters = 50 m and 36 m, respectively. Main net cage and conical bottom heights = 22.5 m and 9 m, respectively. The square elements represent the discretization of the net and are further divided into triangles. Axes dimensions in meters.

20 mm, respectively.  $Sn = 2d/l - (d/l)^2$  was used to determine the twine diameter by using the solidity found by image analysis (0.245) and a realistic half mesh length (20 mm) for a full scale netting. This formula for solidity represents the projected area of the net as an idealized structure consisting of cylinders without excess material in the knots. In effect, this will yield a higher ratio between the twine diameter and half mesh length in the simulations compared to the model tests. This

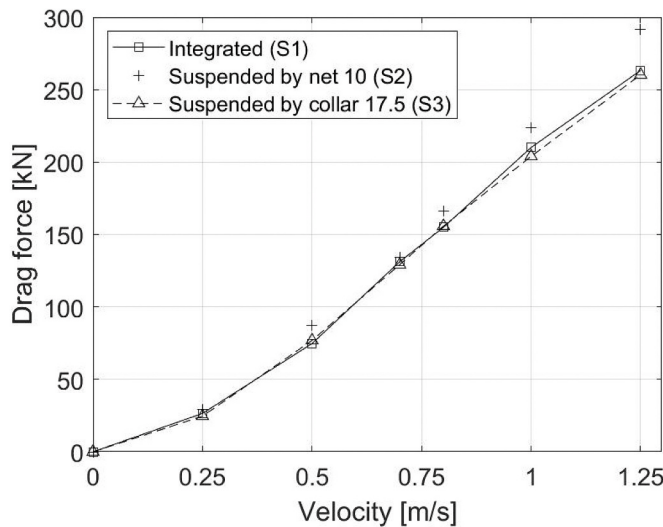


Fig. 10. Model test results for the cylindrical cage considering an integrated bottom ring (squares) suspended by a net with 10-m lines (plus) and a floating collar with 17.5-m lines (triangles).

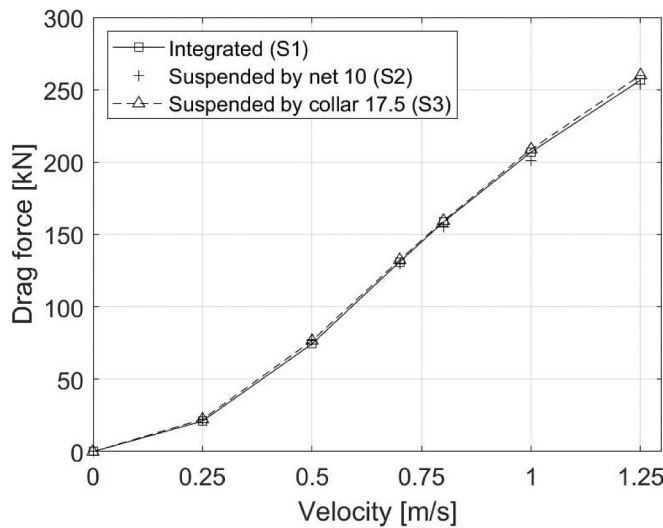


Fig. 11. Simulation results for the cylindrical cage considering an integrated bottom ring (squares) suspended by a net with 10-m lines (plus) and a floating collar with 17.5-m lines (triangles).

relation was used by Kristiansen and Faltinsen (2012) to determine solidity and is used in the numerical method in the present study to conform with the method. The calculated drag coefficient for the net element is dependent on both the solidity and twine diameter. The solidity affects the panel/element drag coefficient by being directly used in the formula, while the twine or mesh bar diameter is used together with the solidity to determine the effective Reynolds number, giving the equivalent drag coefficient for the (presumed) cylindrical mesh bars. The equivalent drag coefficient is used together with the solidity ratio to determine the drag (and lift) coefficient for the net panel. This means that change in solidity have a large effect on the drag coefficient for full scale netting materials. A brief description of how to calculate the drag and lift coefficients on net panels, from Kristiansen and Faltinsen (2012), are as follows: The drag coefficient  $C_D(\theta)$  and lift coefficient  $C_L(\theta)$  for the panel are given as  $C_D(\theta) = c_d(a_1 \cos(\theta) + a_3 \cos(3\theta))$  and  $C_L(\theta) = c_l(b_2 \sin(2\theta) + b_4 \sin(4\theta))$ , where  $\theta$  is the angle between the panel normal vector and the undisturbed incident flow.  $\theta$  varies between 0 and  $\pi/2$ .  $c_d$  and  $c_l$  are the drag coefficient for the panel for  $\theta = 0$  and lift

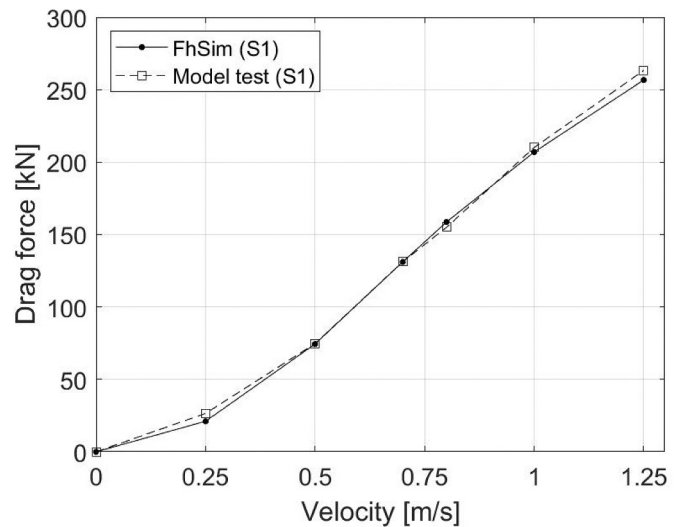


Fig. 12. Integrated bottom ring. Comparison between numerical simulation and model tests.

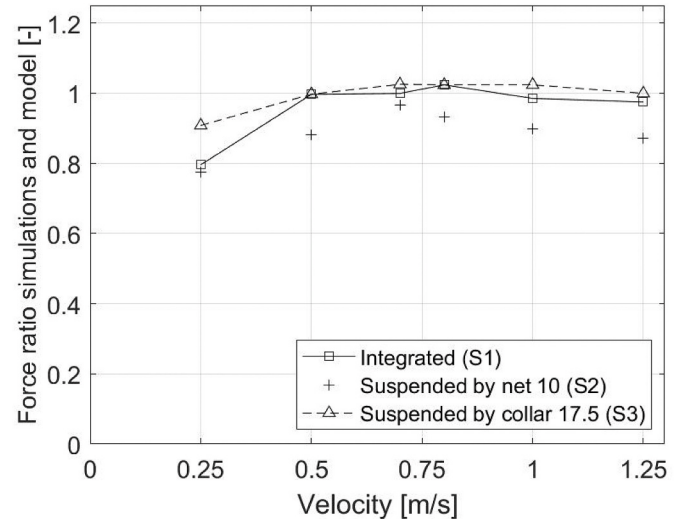
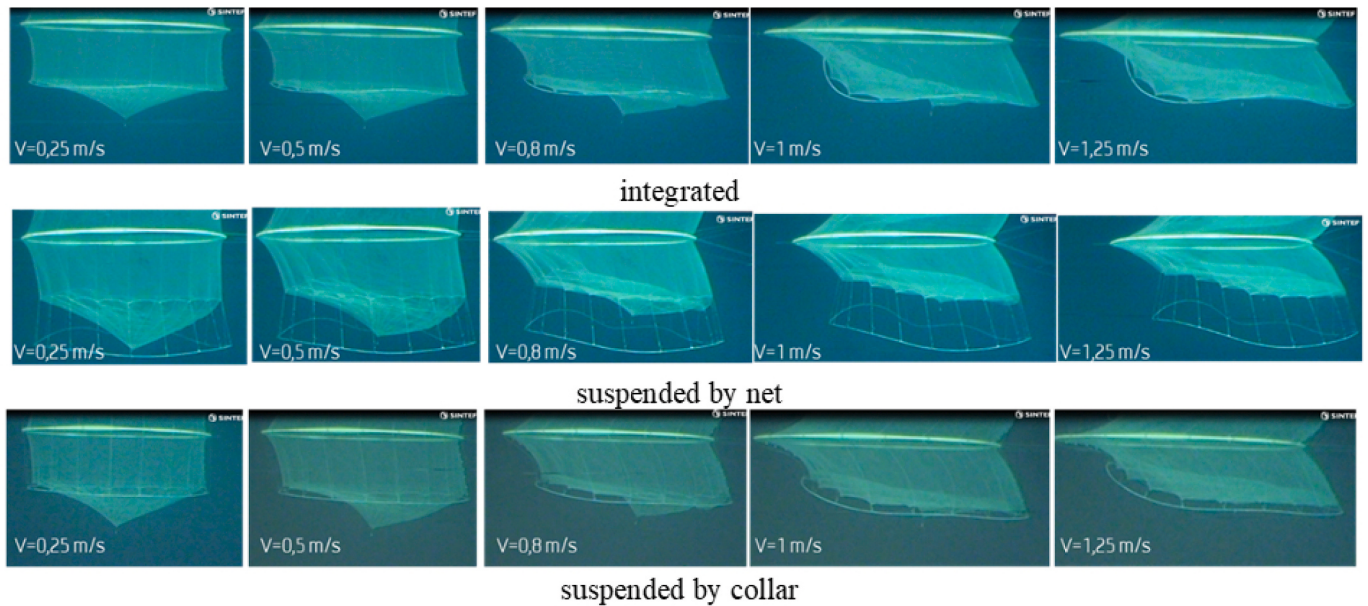


Fig. 13. Drag force from simulations divided by up-scaled values from model tests for the cylindrical cases.

coefficient for  $\theta = \pi/4$ , respectively. Hence, the criterion  $a_1 + a_3 = 1$  must be satisfied while  $b_2 = 1$ .  $c_d$  and  $c_l$  are calculated by first finding the drag coefficient for a circular cylinder  $C_D^{cyl}$  as the function of the Reynolds number.  $C_D^{cyl}$  can be found from experiments or published data, while the Reynolds number is given as  $Re = (d_t \cdot U_{rel}) / (\nu(1 - Sn))$ , where  $d_t$ ,  $U_{rel}$ ,  $\nu$  and  $Sn$  are the twine diameter of the netting, incident relative flow velocity to the panel, kinematic viscosity and netting solidity, respectively. Further,  $c_d$  is given as  $c_d = C_D^{cyl} Sn(2 - Sn) / (2(1 - Sn)^2)$ . The lift coefficient is then found by evaluating the relation between normal and tangential forces on the panel, resulting in  $c_l = c_d(0.5 - \pi / (16 + c_d)) / \sqrt{2}$ . The drag and lift force on each panel is then given as  $F_{D,L}(\theta) = 0.5\rho A C_{D,L}(\theta) U_{rel}^2$ , where  $F_{D,L}(\theta)$  and  $C_{D,L}(\theta)$  are the drag or lift force and drag or lift coefficient, respectively.  $\rho$  is water density while  $A$  is the panel area.

The numerical model in the present study did only use the first harmonic function ( $\cos(\theta)$ ,  $\sin(2\theta)$ ) presented in Kristiansen and Faltinsen (2012) for determining the drag and lift force, giving  $a_1 = b_2 = 1$  and  $a_3 = b_4 = 0$ . Kristiansen and Faltinsen (2012) indicates that  $0 < a_3 < 0.1$  and  $b_4 > 0$ . Setting  $a_3 = b_4 = 0$  results in a possibly



**Fig. 14.** Cylindrical cage deformation considering different suspension rope lengths and main weights.

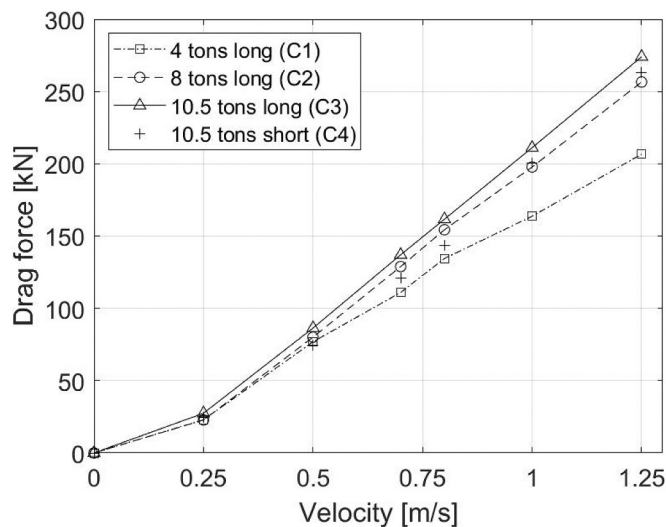


**Fig. 15.** Model test results for the conical cage considering three different central weights (4, 8, and 10.5 metric tons) and two suspension rope lengths (long = 60 m and short = 30 m).

conservative formula with slightly higher drag forces and a shift of the angle for which maximum lift occurs compared with  $0 < a_3 < 0.1$  and  $b_4 > 0$ .

Since only constant water velocity was evaluated, the buoyancy of the floating collar did not influence the drag forces on the net or weight system, and the floating collar was omitted from the numerical setup. The drag forces on the collar alone (obtained through model tests) were subtracted from the model test results of the net cages before comparing them with the numerical results.

### 3. Results and discussion

#### 3.1. Scaling

All results are given as full scale values. Froude scaling was used to convert the model test results to full-scale values with a scale factor of  $\lambda = 25$  (scale 1:25) before comparing them with numerical values

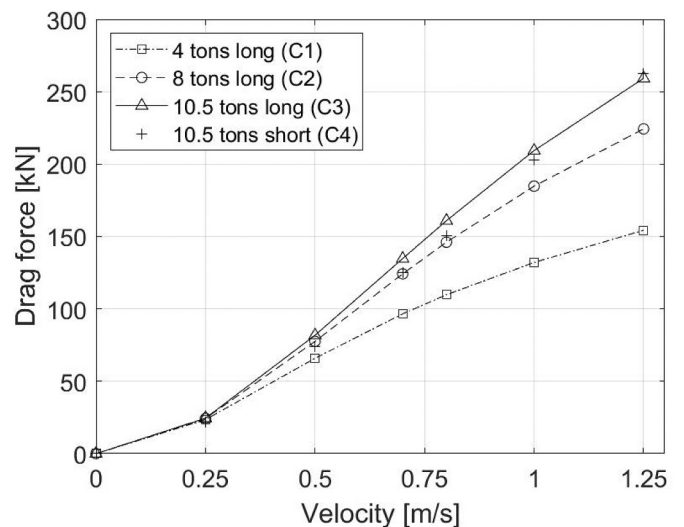


**Fig. 16.** Simulation results for the conical cage considering three different central weights (4, 8, and 10.5 metric tons) and two suspension rope lengths (long = 60 m and short = 30 m).

(simulated in full scale). The main dimensions were scaled with the scale factor ( $\lambda$ ) and velocity with  $\sqrt{\lambda}$ , while weight and forces were scaled as  $1.025\lambda^3$ . The factor 1.025 is due to the difference in water density between the evaluated model and the full-scale model.

#### 3.2. Cylindrical net cage

The model tests of the cylindrical cage did not reveal significant difference in the forces between the integrated bottom ring (suspended in the net, S1 in Table 1) and the bottom ring suspended in the floating collar (S3). However, there was a significant increase in the drag force experienced by the bottom ring suspended 10 m below the cylindrical bottom of the cage (S2) (Fig. 10). In contrast, the simulation results (Fig. 11) did not reveal differences in drag forces between the three cases. Comparison between the model tests and numerical simulations for the integrated bottom ring (S1) are shown in Fig. 12. The ratio between simulation results and experiments (S1–S3) can be found in

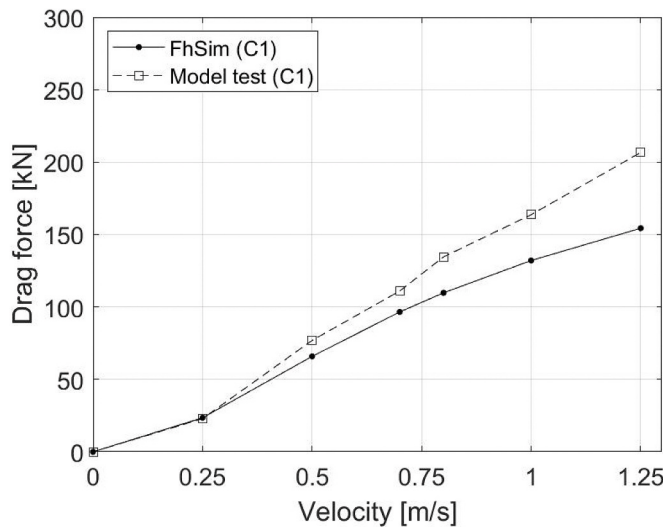


Fig. 17. Comparison between model tests and numerical simulations of conical cage with 4-ton central weight and long suspension ropes (60 m).

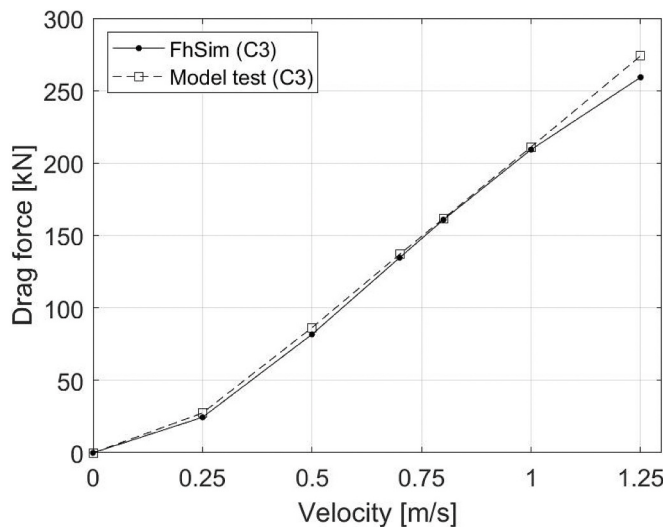


Fig. 18. Comparison between model tests and numerical simulations of conical cage with 10.5-ton central weight and long suspension ropes (60 m).

Fig. 13. The cases with an integrated bottom ring (S1) and the bottom ring suspended in the floating collar (S3) were similar in the sense that the vertical position of the bottom ring in relation to the net are comparable. The length of the ropes connecting the collar-suspended bottom ring to the net are relatively short, and the effect of the bottom ring on the net when subjected to currents may have been comparable to the case with the integrated bottom ring. The main difference between the cases is which part of the net structure supports the weight of the bottom ring. The net supports the entire weight of the bottom ring in the integrated and net suspended cases, whereas a larger portion of the weight presumably is supported by the floating collar in the case where the bottom ring is connected to the floating collar. However, when velocity and, subsequently, the loading and deformations on the cage increase for the floating collar-supported setup, a larger portion of the bottom ring may be supported by the net. Pictures from the model tests are shown in Fig. 14.

### 3.3. Conical net cage

For the conical net cage, both the model tests and simulation results

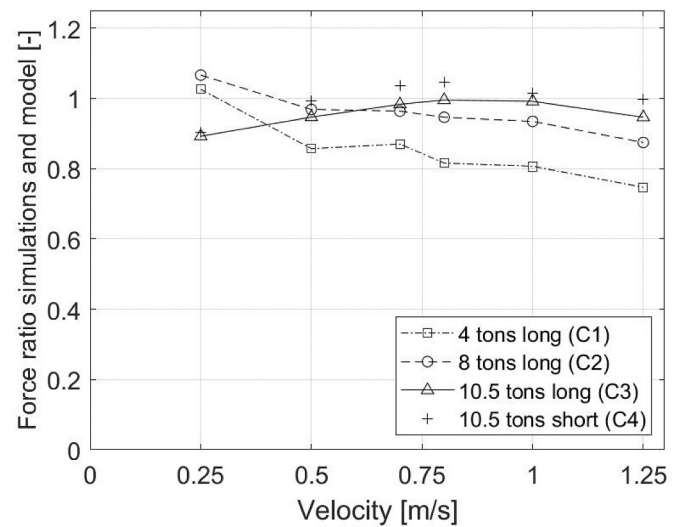


Fig. 19. Drag force from simulations divided by up-scaled values from model tests for the conical cases.

showed, not surprisingly, dependency on the magnitude of the central weight. However, whereas the model tests indicated a moderate reduction in drag forces when the weight is reduced (Fig. 15), the simulations showed a much larger decrease (Fig. 16).

Drag forces on the cone-shaped cage seem to be reduced by a small amount (model test results) when shortening the length of the lines. The central load weights are equal between the cases with long and short lines, indicating that both geometry and tension in the lines affect the deformation of the net cage (Fig. 15). Evaluating a static case without current implies that tensions in the lines holding the central weight will increase with decreasing length of the lines due to the higher angle of the line with respect to the vertical. The comparison of the two cases implies that a larger angle (shorter lines) results in larger inward radial forces compared with the long line case. The simulations partly support this assessment but show approximately equal drag force at  $1.25 \text{ ms}^{-1}$  (Fig. 16).

The comparison of drag forces between the experiments and numerical simulations for the cone-shaped cages (Fig. 17, Fig. 18 and Fig. 19) show that for the 4-ton case (C1, Fig. 17) the numerical results are, with the exception of 0.25 m/s, lower than the experiments results for all velocities. The largest difference between numerical simulations and experiments occur for 1.25 m/s. For 0.8 m/s and higher C1 shows the largest difference between the numerical simulations and the experiments for all the cone-shaped cases (Fig. 19). The 8-ton case (C2) has, similar to C1, a decreasing ratio between numerical results and experiments for increasing velocity. For 0.5 m/s and higher velocities numerical results for C2 compares better with experiments than C1. For 0.7 m/s and higher velocities numerical results for C3 (10.5-ton, Fig. 18) compare best with experiments among the three conical cases with similar geometry (C1, C2 and C3). For C3 the numerical results were closest to the experiment results for 0.7 m/s to 1.0 m/s. The largest underestimations of forces for C3 were found for 0.25 m/s, 0.5 m/s and 1.25 m/s. Numerical results for the 10.5 ton short lines case (C4) compared best with experiments for 0.5 m/s, 1.0 m/s and 1.25 m/s, while the drag force was overestimated compared with experiments for 0.7 m/s and 0.8 m/s. For full scale velocities of 0.8 m/s and higher the results indicate that increasing the central bottom weight results in better comparison between simulations and experiments with regards to drag forces. It also indicates that the numerical method is able to reproduce loads and deformations up to a certain global deformation level. Evaluation of deformation is more complex than simply comparing vertical displacement of the bottom part of the net. For a net cage with small or negligible global deformation, large parts of the

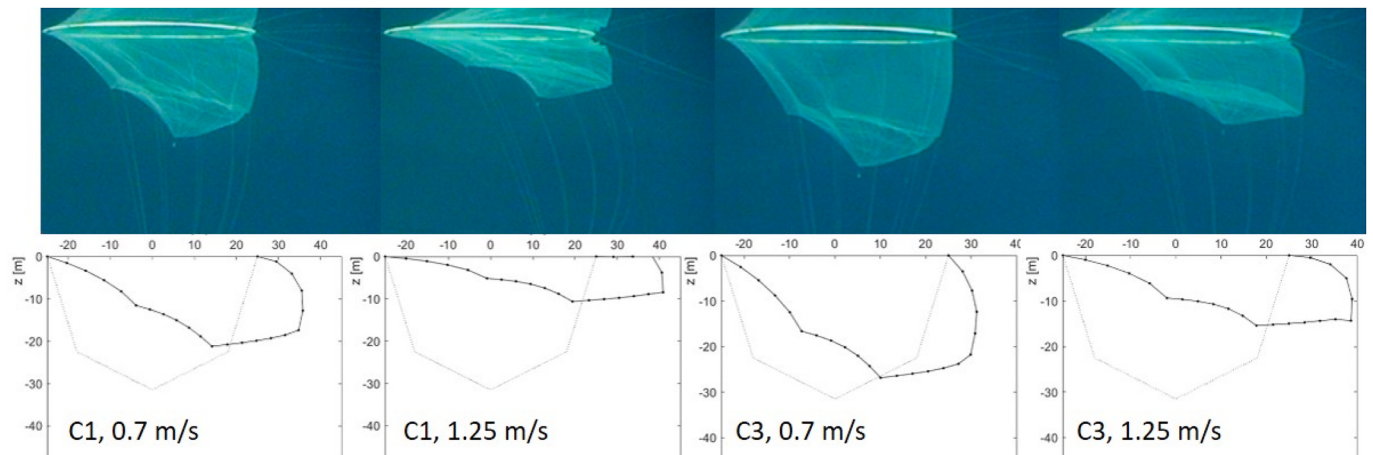


Fig. 20. Deformations from model tests (top) and numerical simulations (bottom) for C1 and C3 for velocities of 0.7 m/s and 1.25 m/s.

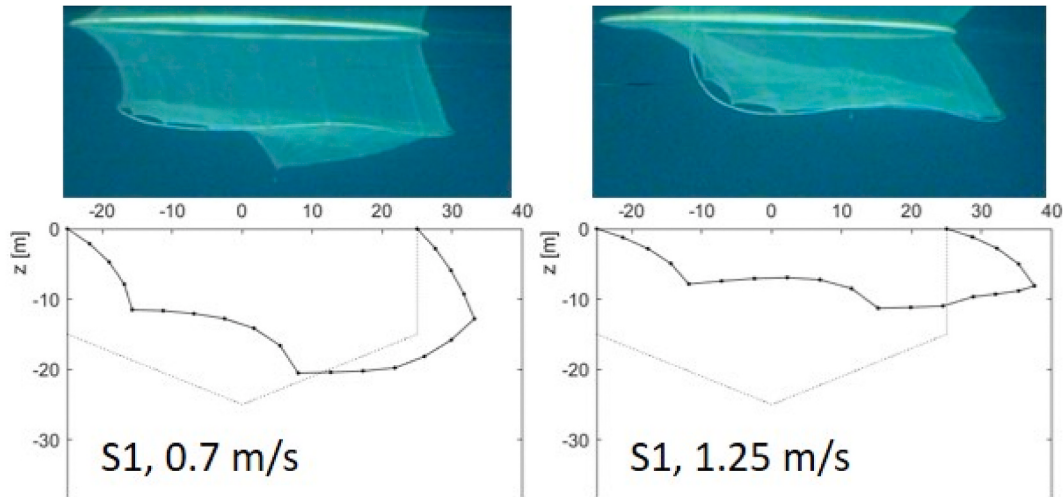


Fig. 21. Deformations from model tests (top) and numerical simulations (bottom) for S1 for velocities of 0.7 m/s and 1.25 m/s.

netting will still have a medium or low angle of attack. This is prevalent on the sides of the cage where the panel planes are parallel to the incident current velocity. With high currents and possibly large global deformations, the numbers of panels with small angles of attack will increase; thus, discrepancies with respect to low angles of attack will most likely be larger for large global deformations.

One effect seen in the numerical model of the conical net is that a portion of the rear top part of the net is lifted towards the water surface. When this happens, many of the panels orient themselves horizontally and parallel to the velocity vector. This effect was more present for the 4-ton bottom weight than for the 10.5-ton bottom weight (Fig. 20), while it was not observed to this degree for the cylindrical cages (Fig. 21). This may be a physical effect or an effect of the structural modeling arising when large forces cause the downstream part of the net to lift, thereby also causing the top rear part of the net to lift and become flat and parallel with the velocity vector. This effect, however, is not observed visually in the model tests, where a fold occurred in the net below the surface on the downstream side of the net (Figs. 20 and 22). The force estimated for each net panel in the numerical model tends toward zero for small angles of attack, yet there still may be a force contribution from that part of the net in the physical model, which might partly explain why the simulation is underestimating the drag for the 4-ton bottom weight case.

#### 3.4. Wake effect

When modeling the forces affecting a net cage, the reduced velocity or wake behind the upstream parts of the net must be considered. Kristiansen and Faltinsen (2012) used the formulation from Løland (1991) where the rear (downstream) side of the net is subjected to a reduced velocity due to blockage from the fore (upstream) part of the net. This approach was also applied in the numerical model used in this work, using the same formulation for velocity reduction. This means that the entire downstream part of the net experiences the same reduced velocity. An earlier work (Patursson et al., 2010) suggests that velocity reduction is dependent on the orientation (angle of attack) of preceding panels. Another factor is the possibility of change in the flow pattern (e.g., direction) due to the presence of the net (Gansel et al., 2012), which can modify the angles of attack on both the upstream and downstream parts of the net. When comparing the measured velocity at the center of the cage, it was found that it rarely matched with the theoretical velocity. The measured velocities are presented as a velocity reduction factor,  $r = U_1/U_\infty$  in Fig. 23 and Fig. 24, where  $(U_1, U_\infty)$  are the velocities after passing through one net panel and undisturbed velocity, respectively. In general, the measured values were closer to the theoretical values at higher flow velocities and matched better overall for the conical cages than for the cylindrical cages. The velocity reduction was on average higher than predicted by theory, and there was no definite rule to whether measured velocity reduction would indicate how well

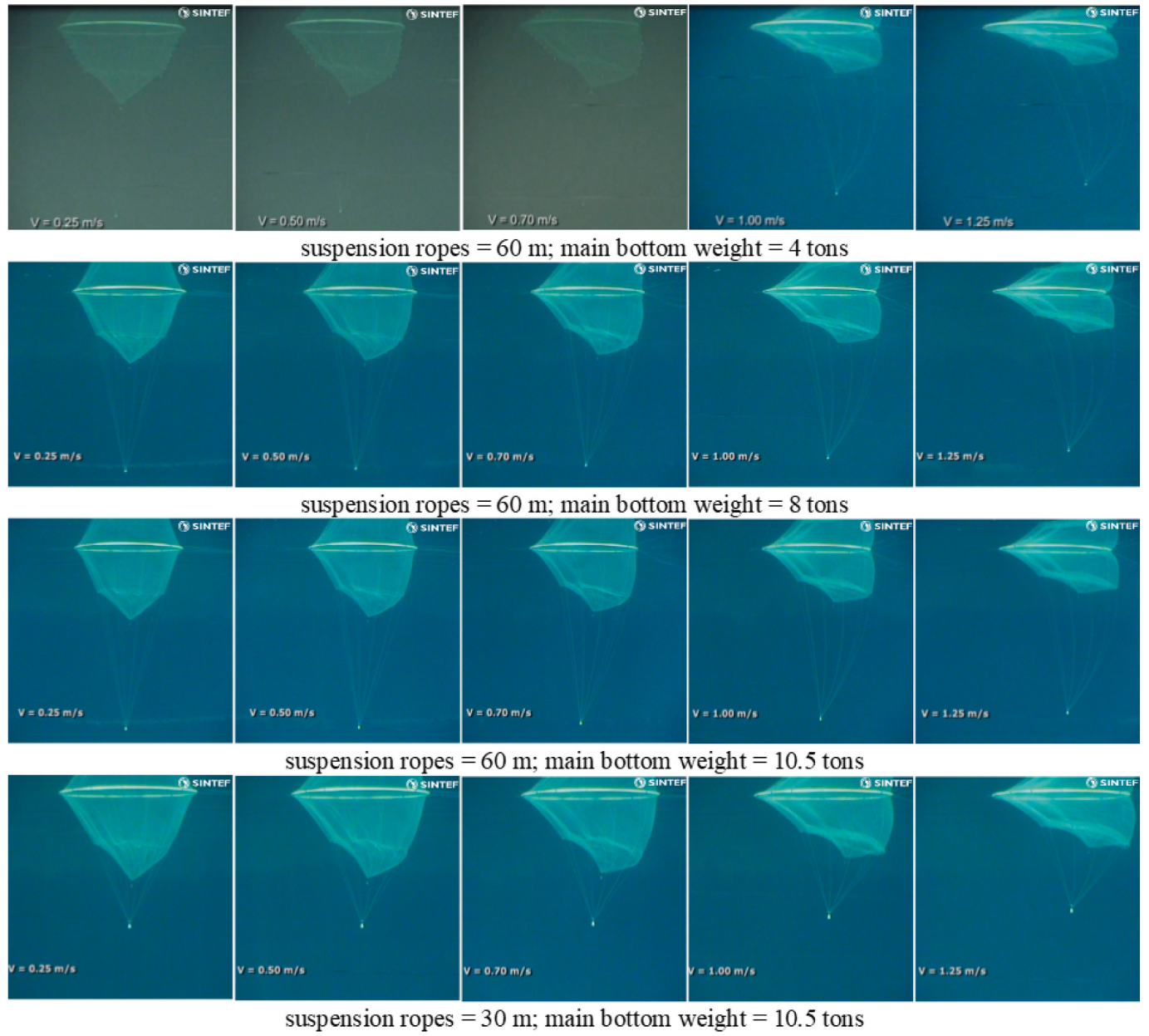


**Fig. 22.** Conical cage deformation considering different suspension rope lengths and main weights.

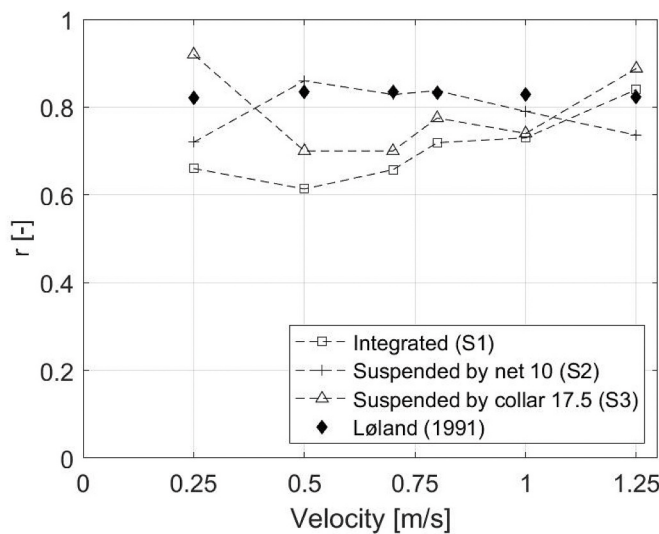


**Fig. 23.** Velocity reduction factor in the middle of the cage for the cylindrical cases.

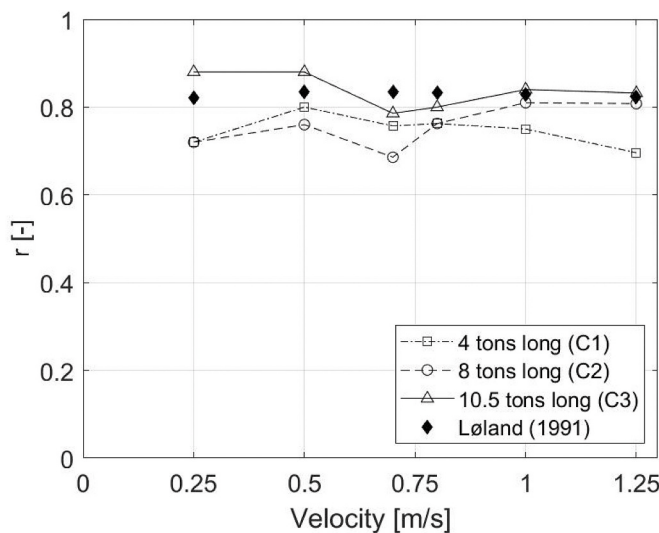


**Fig. 24.** Velocity reduction factor in the middle of the cage for the conical cases.

model tests and numerical simulations would compare in terms of total drag forces. The exception was the conical cage with long suspension ropes and a 10.5-ton weight (C3), for which both the measured drag forces and velocity in the center of the cage matched well with numerical results. As mentioned, the measured velocities compared better with the theoretical velocities at higher velocities, with the exception of the 4-ton conical case (C1) and the cylindrical cage with the bottom ring suspended 10 m below the main part of the cage (S2). The latter were also the cases where the numerical results differed the most from the measured drag forces.

### 3.5. Uncertainties

As the model tests were performed on model-scale netting with a small twine diameter, there may be flow pattern effects not accounted for by the numerical model. Other works on net panels (Zhan et al., 2006; Patursson et al., 2010) show that the drag coefficient may depend on Reynolds number. The relatively small velocities in model scale combined with the small twine diameter in the model net may affect

drag coefficients for the model net due to low Reynolds numbers. This may also have an effect on flow velocities through the cage. As both the velocities and the measured forces in model scale were relatively low, measuring accuracy may be a source of uncertainty, especially for the lowest velocities tested. Solidity measurements may also be a source for uncertainty. The largest differences between model tests and simulations occurs for 0.25 m/s for the cylindrical cages (S1–S3), while this is only the case for the two conical cages with the 10.5 ton center weight (C3 and C4). The ratio between simulated drag forces and measured drag forces generally decrease with increasing velocity for the conical 4- and 8-ton cases (C1 and C2), respectively.

### 4. Conclusion

The results for the model tests and numerical simulations were very similar for the cylindrical net cages with the bottom ring integrated (fully supported) in the net and supported by the floating collar by lines (traditional setup) and for the conical net cages with a heavy central load (10.5 tons). The simulations of the cylindrical cage with the bottom ring supported by the net and 10-m lines and the conical cage with an 8-ton central weight indicated a drag force 87% of that measured in the model tests at a flow velocity of 1.25 m/s. For a complex structure such as a net cage, these results are not unexpected, but compared to the other cylindrical cases, they still indicate a significant underestimation of the forces. Numerically, the three cylindrical cases experienced similar drag forces, while the model tests showed noticeably higher forces on the net-supported bottom ring with 10-m long lines. Adequate explanations for this discrepancy were not found. The results of the simulations of the conical net with an 8-ton central weight were adequate compared with the model tests (87%), whereas the simulations of the 4-ton case had a drag force 75% of that found in the model tests for 1.25 m/s. For the conical net cages, lower weights seemed to decrease the performance of the numerical model. This may partly be due to increased global deformations of the net cage and discrepancies between simulations and model tests in local deformation at the rear top part of the net for high flow velocities. Furthermore, it is possible that low Reynolds numbers in the model tests affect the results.

### CRediT authorship contribution statement

**Per Christian Endresen:** Formal analysis, Investigation, Methodology, Project administration, Software, Validation, Visualization, Writing - original draft, Writing - review & editing. **Pascal Klebert:** Data curation, Formal analysis, Funding acquisition, Investigation, Methodology, Project administration, Validation, Visualization, Writing - original draft.

### Declaration of competing interest

The authors declare that they have no known competing financial interests or personal relationships that could have appeared to influence the work reported in this paper.

### Acknowledgements

The study presented in this paper was carried out as part of the research projects funded by The Research Council of Norway: “Towards Sustainable Fish Farming at Exposed Marine Sites” (SUSTAINFARMEX: 210794/O70), “Aquaculture operations with reliable flexible shielding technologies for prevention of infestation in offshore and coastal areas” (FLEXAQUA: 284361/E40) and by the research project “Water Currents in fish farms at site scale” from the RACE research grant program financed by SINTEF Ocean, Norway.

## References

- Balash, C., Colbourne, B., Bose, N., Raman-Nair, W., 2009. Aquaculture net drag force and added mass. *Aquacult. Eng.* 41 (1), 14–21. ISSN 0144-8609.
- Endresen, P., Birkevold, J., Føre, M., Fredheim, A., Kristiansen, D., Lader, P., 2014. Simulation and validation of a numerical model of a full aquaculture net-cage system. In: ASME. Proceedings of the International Conference on Offshore Mechanics and Arctic Engineering, Volume 7: Ocean Space Utilization. Professor Emeritus J. Randolph Pauling Honoring Symposium on Ocean Technology: V007T05A006. <https://doi.org/10.1115/OMAE2014-23382>.
- FAO, 2018. The State of World Fisheries and Aquaculture 2018: Meeting the Sustainable Development Goals. Rome. Food and Agriculture Organization of the United Nations. Licence: CC BY-NC-SA 3.0 IGO.
- Gansel, L.C., Mc Climans, T.A., Myrhaug, D., May 31, 2012. Average flow inside and around fish cages with and without fouling in a uniform flow. ASME. J. Offshore Mech. Arct. Eng. November 2012 134 (4). <https://doi.org/10.1115/1.4006150>, 041201.
- Klebert, P., Lader, P.F., Gansel, L., Oppedal, F., 2013. Hydrodynamic interactions on net panel and aquaculture fish cages: A review. *Ocean Eng.* 58, 260–274.
- Kristiansen, T., Faltinsen, O.M., 2012. Modelling of current loads on aquaculture net cages. *J. Fluid Struct.* 34, 218–235.
- Li, Y.C., Zhao, Y.P., Gui, F.K., Teng, B., 2006. Numerical simulation of the hydrodynamic behaviour of submerged plane nets in current. *Ocean Eng.* 33, 2352–2368. <https://doi.org/10.1016/j.oceaneng.2006.11.013>.
- Løland, G., 1991. Current Force on and Flow through Fish Farms. Dr.Ing Dissertation, Division of Marine Hydrodynamics. The Norwegian Institute of Technology.
- Moe, H., Fredheim, A., Hopperstad, O.S., 2010. Structural analysis of aquaculture net cages in current. *J. Fluid Struct.* 26 (3), 503–516.
- Patursson, Ø., Swift, M.R., Tsukrov, I., Simonsen, K., Baldwin, K., Fredriksson, D.W., Celikkol, B., 2010. Development of a porous media model with application to flow through and around a net panel. *Ocean Eng.* 37 (2–3), 314–324. ISSN 0029-8018.
- Priour, D., 1999. Calculation of net shapes by the finite element method with triangular elements. *Commun. Numer. Meth. Engng.* 15, 755–763. [https://doi.org/10.1002/\(SICI\)1099-0887\(199910\)15:10<755::AID-CNM299>3.0.CO;2-M](https://doi.org/10.1002/(SICI)1099-0887(199910)15:10<755::AID-CNM299>3.0.CO;2-M).
- Reite, K., Fore, M., Aarsæther, K., Jensen, J., Rundtop, P., Kyllingstad, L.T., Endresen, P., C., Kristiansen, D., Johansen, V., Fredheim, A., et al., 2014. FHSIM — time domain simulation of marine systems. In: ASME. International Conference on Offshore Mechanics and Arctic Engineering, 8A. Ocean Engineering:V08AT06A014.
- Su, B., Reite, K., Fore, M., Aarsæther, K.G., Alver, M., Endresen, P., Kristiansen, D., Haugen, J., Caharija, W., Tsarau, A., 2019. A Multipurpose Framework for Modelling and Simulation of Marine Aquaculture Systems. In: ASME. International Conference on Offshore Mechanics and Arctic Engineering. OMAE2019, Glasgow, Scotland. June 9–14, 2019.
- Zhan, J.M., Jia, X.P., Li, Y.S., Sun, M.G., Guo, G.X., Hu, Y.Z., 2006. Analytical and experimental investigation of drag on nets of fish cages. *Aquacult. Eng.* 35 (1), 91–101.
- Zhao, Y.-P., Bi, C.-W., Chen, C.-P., Li, Y.-C., Dong, G.-H., 2015. Experimental study on flow velocity and mooring loads for multiple net cages in steady current. *Aquacult. Eng.* 67, 24–31. ISSN 0144-8609.